Distinguishing between benign and malignant melanocytic nevi by in vivo multiphoton microscopy

Mihaela Balu[a], Kristen M. Kelly[b], Christopher B. Zachary[b], Ronald M. Harris[b], Tatiana B. Krasieva[a], Karsten König[c,d], Anthony J. Durkin[a], Bruce J. Tromberg[a]

[a] Laser Microbeam and Medical Program, Beckman Laser Institute, University of California, Irvine, Irvine, CA, 92612

[b] Department of Dermatology, University of California, Irvine, CA, 92697

[c] JenLab GmbH, Schillerstrasse 1, Jena, Germany

[d] Department of Biophotonics and Laser Technology, Saarland University, Saarbrücken, Germany

Conflict of interest

Karsten König is cofounder of JenLab GmbH.

Abstract. Monitoring of atypical nevi is an important step in early detection of melanoma, a clinical imperative in preventing the disease progression. Current standard diagnosis is based on biopsy and histopathological examination, a method that is invasive and highly dependent upon the physician's experience. In this work, we employed a clinical multiphoton microscope to image in vivo and non-invasively melanocytic nevi at three different stages: common nevi without dysplastic changes, dysplastic nevi with structural and architectural atypia, and melanoma. We analyzed multiphoton microscopy (MPM) images corresponding to 15 lesions (5 in each group) both qualitatively and quantitatively. For the qualitative analysis, we identified the morphological features characteristic of each group. MPM images corresponding to dysplastic nevi and melanoma were compared with standard histopathology in order to determine correlations between tissue constituents and morphology and to evaluate whether standard histopathology criteria can be identified in the MPM images. Prominent qualitative correlations included the morphology of epidermal keratinocytes, the appearance of nests of nevus cells surrounded by collagen fibers, and the structure of the epidermal-dermal junction. For the quantitative analysis, we defined a numerical "multiphoton melanoma index (MMI)" based on 3D in vivo image analysis that scores signals derived from two-photon excited fluorescence, second harmonic generation, and melanocyte morphology features on a continuous 9-point scale. Indices corresponding to common nevi (0–1), dysplastic nevi (1-4) and melanoma (5-8) were significantly different ($p<0.05$), suggesting the potential of the method to distinguish between melanocytic nevi in vivo.

INTRODUCTION

Over the past 10 years of available data (1999-2008), cancer mortality rates have declined by more than 10% in men and women (1), while the mortality rate for melanoma reportedly increased by 5.5% in men and remained stable in women (2). This is most likely due to an increase in the incidence of melanoma compared to other types of cancers (1), and to diagnosis at a late, incurable stage. Early detection is critical for good prognosis and successful treatment of melanoma. (3)

Recently, non-invasive optical imaging technologies based on laser-scanning microscopy have emerged as promising tools for real time, *in situ* imaging of skin lesions with the potential to overcome current diagnostic limitations. These limitations are related to: 1) the dermatologist's decision about the necessity of the biopsy after visual inspection based on dermoscopy and ABCDE rule (Asymmetry, Border Irregularity, Color variegation, Diameter>6mm, Evolving) (4); 2) the dermatopathologist's diagnosis decision based on a series of histological criteria. Consequently, this diagnosis method, subjective and highly dependent upon the physician's experience, creates the problems of false-negative diagnosis, which delay diagnosis and treatment, and of false-positive diagnosis, which lead to unnecessary biopsies and treatments, emotional trauma and increased medical costs. The false-negative and false-positive rates for melanoma diagnosis are reported to be 10-50% (5, 6) and 40-80% (6, 7), respectively. Techniques such as reflectance confocal microscopy (8) and multiphoton microscopy (9) were used in studies aiming to improve the accuracy of dermatologist's decision to perform a biopsy while pump-probe microscopy (10) and fluorescence lifetime microscopy (11) have been used to target limitations related to decisions by dermatopathologists.

Multiphoton microscopy (MPM) is a laser-scanning microscopy technique that relies on nonlinear light-matter interactions such as two-photon excited fluorescence (TPEF) and second harmonic generation (SHG) to achieve 3D images with sub-micron resolution. These contrast mechanisms produce images of endogenous biomolecules in the tissue, without using specific fluorescent labels. In MPM, the main sources of fluorescence are reduced nicotinamide adenine dinucleotide (NADH), flavin adenine dinucleotide (FAD), keratin, melanin, collagen, and elastin fibers while SHG is used to visualize collagen fibers in the dermis.

MPM has recently been used to establish sensitivity and specificity criteria for melanoma diagnosis (12). These criteria were identified based on evaluation of distinguishing characteristics, measured using MPM on both *in vivo* and *ex vivo* samples, linked to morphological changes in melanoma relative to benign nevi and normal (control) skin. Benign nevi can be common (without dysplasia) or dysplastic. Dysplastic nevi and their MPM features have not been described in previous studies. In the pilot study presented here, we expand previous measurements by using MPM *in vivo* to identify characteristic features of melanocytic nevi at three different stages: common nevi without dysplastic changes, dysplastic nevi with structural and architectural atypia, and melanoma. A major focus of this work is to evaluate, for the first time, possibility to distinguish between melanoma and dysplastic nevi, a common clinical challenge, by establishing quantitative diagnostic criteria based on *in vivo* MPM imaging using novel quantitative diagnostic criteria.

MPM images corresponding to dysplastic nevi and melanoma are compared with standard histopathology in order to identify correlations between tissue constituents and morphology and to evaluate whether standard histopathology criteria can be identified in the MPM images. Several histopathologic features characteristic of common nevi, dysplastic nevi

and melanoma are expected to be identified in the MPM images. For example, melanocytic nevi are composed of nevus cells, which, even though they are basically identical to melanocytes, differ from melanocytes by being arranged in clusters, or "nests" and by not showing dendritic processes (13). The nests are usually confined at the tips of the rete ridges (14). They are visualized in the MPM images as clusters of bright cells surrounded by collagen fibers at the bottom of EDJ.

Dysplastic nevi are characterized by cytological atypia (variation in size and shape of nuclei) and architectural disorder not amounting to melanoma in situ (13). Architectural disorder includes lentiginous hyperplasia (proliferation of nevus cells either singly or as nests along the basal layer of epidermis) and nests that are irregular in both shape and distribution and not confined to the tips of the rete ridges. They are visualized in the MPM images as clusters of bright cells that are not fully surrounded by collagen fibers and located along the EDJ.

There are several subtypes of melanoma. Their features have differences and similarities, but generally the following are suggestive of malignancy: presence of melanocytes within the upper portion of the epidermis singly or in groups (Pagetoid spread); irregular junctional activity (atypical melanocytes, architectural disorder); and invasion of tumor cells into the dermis (13, 14).

We assessed qualitatively the presence of these features in the *in vivo* MPM images corresponding to 15 lesions identified in 14 patients. We introduced three parameters related to TPEF, SHG and melanocyte morphology in order to quantify the histopathologic features identified in the MPM images. These parameters have been combined to obtain a numerical "multi-photon melanoma index (MMI)". The MMI scale ranges from 0-9, where 0 and 9 represent the lowest and highest probability of melanoma, respectively. The MMI is a first

attempt to develop a quantitative index based on *in vivo* image parameters that capture multiple relevant contrast elements unique to intrinsic-signal non-linear optical microscopy.

MATERIALS AND METHODS

MPTflex clinical tomograph

The laser-scanning based clinical multiphoton tomograph, MPTflex (JenLab GmbH, Germany) consists of a compact, turn-key femtosecond laser (MaiTai Ti:Sappire oscillator, sub-100 fs, 80 MHz, tunable 690-1020 nm; Spectra Physics, Mountain View, CA), an articulated arm with near-infrared optics, and beam scanning module. The system has two photomultiplier tube (PMT) detectors employed for parallel acquisition of TPEF and SHG signals. A customized metallic ring taped on the subject's skin attaches magnetically to the objective holder in the articulated arm, minimizing motion artifacts. The excitation wavelength used for this study was 790 nm. The TPEF signal was detected over the spectral range of 410nm-650nm while the SHG signal was detected over a narrow spectral bandwidth 385nm-405nm through emission filters placed in the TPEF and SHG detection channels, respectively. We used a Zeiss objective (40X, 1.3NA, oil immersion) for focusing into the tissue.

Study design

We imaged 15 melanocytic nevi (5 common nevi, 5 dysplastic nevi and 5 melanoma) in 14 patients. All *in vivo* measurements were conducted according to an approved institutional protocol with written informed consent obtained from all patients. The 15 lesions were distributed in 6 primary locations for all patients, including back (4), arms (4), legs (1), chest (1), abdomen (3) and face (2). MPM measurements were performed on lesion sites as well as on

adjacent normal skin. Optical sections of about 200x200 μm^2 at different depths ranging from 0 to about 200 μm (5 μm steps) were obtained. The time required for each optical section was 6 s. As the optical section is limited to a small scan field, the overall investigation of the lesion required the acquisition of several image stacks of different skin sites. We acquired about three image stacks for each lesion. All lesions clinically diagnosed as dysplastic nevi and melanoma by board certified dermatologists (KMK and CBZ) were biopsied and diagnosed by a dermatopathologist (RMH), using standard H&E histopathology. For the qualitative analysis, we compared MPM and histologic images in order to determine whether H&E histopathology hallmarks could be correlated with structures in *in vivo* MPM images. Quantitative methods are described below.

Image analysis

All images were processed using ImageJ (15). For the quantitative analysis we wrote macros for automatic measurement of key parameters characteristic of TPEF and SHG images. TPEF images were also used to identify and calculate the number of melanocytic dendrites. A composite "multi-photon melanoma index (MMI)" was linearized on a 0-9 scale.

For the ***TPEF contrast*** we used the raw TPEF images to calculate the ratio (F) between the spatial standard deviation and the mean pixel intensity for each TPEF image in a z-stack corresponding to the epidermal-dermal junction (EDJ).

$$F = \frac{\sigma_{Fl}}{< I >}$$

where σ_{Fl} is the spatial standard deviation of fluorescence signal intensity and <I> the mean pixel intensity in the TPEF image. For each lesion, F ratios were calculated over 5 consecutive image

planes (spanning a total of 20 μm in depth), starting with the image of the basal layer in each acquired stack and going down into the EDJ. We considered the EDJ starting at the location where the collagen structure in the top of the papilla was visualized. The basal layer was defined as the first cell layer above the EDJ.

A mean F value was calculated for each lesion. The mean represents the average F value over the TPEF images analyzed in all stacks of the lesion.

Parameter **F** is related to epidermal features assessed qualitatively by histopathology, such as lentiginous hyperplasia and Pagetoid spread. By its definition, it measures the degree of pixel intensity homogeneity in the MPM image.

For the ***SHG contrast***, the SHG images were converted to 8-bit images and subsequently to binary images by using the automatic thresholding function in ImageJ (16). The automatic thresholding procedure was suitable for our analysis because the signal-to-background ratio (SBR) of the SHG images was high. The average SBR for each of the SHG images included in the analysis was at least 10:1 and typically averaged greater than 20:1. The "bright pixels" were defined as the pixels of value 1 in the binary images. We defined the density of the bright pixels by the ratio between the number of bright pixels and total number of pixels in one image. The density of bright pixels was calculated for each image in a z-stack of 8 consecutive image planes (spanning a total of 35 μm in depth), starting with the first SHG image of the EDJ. For each stack, a parameter S was defined as:

$$S = \frac{\sigma_{SHG}}{< \rho >}$$

where σ_{SHG} is the standard deviation and $\langle\rho\rangle$ the mean density of bright pixels in the binary SHG images of the stack. A mean S value was calculated for each lesion. The mean represents the average S value over all the stacks of SHG images of the lesion.

Parameter **S**, by its definition, is a measurement of the change in collagen across the EDJ and therefore, a measurement of histopathology features such as irregular nests of nevus cells along the basal layer, erosion of the junction, and invasion of melanocytes into the dermis. A large S reflects a rapid increase in the collagen amount from the top of the dermal papillae to deeper layers in the papillary dermis. A small S value reflects a slower increase in collagen content across the junction, which is due to the presence of cells in the papillary dermis; typically nevus cells from the sides of the rete ridges in dysplastic nevi and melanoma cells in melanoma lesions. A larger volume at the EDJ would comprise more information for image analysis, but for dark, highly pigmented nevi, TPEF and SHG signals diminish with depth due to high absorption and scattering. Stacks of 20 μm and 35 μm total thickness for TPEF and SHG images respectively, proved to contain relevant information in all analyzed lesions.

To determine ***melanocytic dendrite density***, we used the NeuronJ plug-in (17) in ImageJ for tracing and counting of melanocytic dendrites in the TPEF images corresponding to spinosum and granulosum epidermal layers. We calculated a density parameter D, which was defined as the number of melanocytes in a stack volume.

$$D = \frac{N}{V}$$

where N is the number of melanocytic dendrites in the stratum spinosum and granulosum of the epidermis and V is the volume (the image area x the thickness of the epidermis from the stratum corneum to the basal layer). A mean D value was calculated for each lesion. The mean represents the average D value obtained from melanocytic dendrites counted by two independent observers.

Parameter **D** represents a measurement of the density of melanocytic dendrites in upper epidermal layers. A high density number is a hallmark of melanoma, but a limited number of melanocytic dendrites is allowed in the stratum spinosum of the epidermis in dysplastic nevi (18). Parameter D was introduced in order to address this ambiguity.

RESULTS

Typical MPM images of normal pigmented skin are shown in Figure 1. MPM features are characterized by normal morphology and architecture of keratinocytes in the epidermal layers, a clearly delineated epidermal-dermal junction (EDJ), and the presence of normal collagen and elastin fibers in the dermis. Pigmented keratinocytes are present in the basal layer. They appear as bright fluorescent cells along the EDJ due to their melanin content. Blood vessels can be visualized in the dermis. These features can be noted in both horizontal sections (X-Y scan) and the corresponding cross-sectional (X-Z scan) images.

We performed MPM imaging of pigmented lesions in three stages: 1) common melanocytic nevi without dysplastic changes, 2) dysplastic nevi with structural and architectural atypia, and 3) melanoma. MPM images were analyzed qualitatively by identifying the morphological features characteristic of each group of lesions. Quantitative analysis consisted of, measuring the parameters F, S and D, which are related to signals from TPEF, SHG, and melanocytic dendrites, respectively *(see Materials and Methods)*.

Melanocytic nevi (without dysplastic changes)

We imaged 5 melanocytic nevi in 5 patients (common nevi without dysplastic changes), clinically diagnosed as junctional or compound nevi.

The MPM features of melanocytic nevi were characterized by normal morphology of keratinocytes of the epidermal layers and well-defined nests of nevus cells surrounded by collagen fibers at the EDJ and in the dermis. Three melanocytic nevi imaged showed elongated rete ridges (Figure S1). Occasional melanocytic dendrites were visualized in the basal layer, but no dendrites were imaged in the upper epidermal layers of the common nevi imaged in this study. Melanocytic nevi were not biopsied, but the features identified by the MPM imaging were in good correlation with features generally identified by histopathology in junctional and compound nevi (14).

The mean of F values for common nevi ranged between 0.86 and 1.07. The mean of S values ranged between 0.42 and 0.6. The mean of D values was zero for all common nevi (Table 1).

Figure 2 shows representative MPM images of a compound nevus at different depths. Nevus cells are visualized as bright disk-like or oval cells among pigmented basal cells (Figure 2b). Pigmented basal cells and melanocytes are also present in pigmented skin. Nevus cells can be distinguished from pigmented basal cells and melanocytes by examining cellular morphology and organization. Nevus cells appear to be identical to melanocytes, but differ because they are generally arranged in clusters, or “nests” and do not show dendritic processes (13). Thus, as individual cells, nevus cells and pigmented keratinocytes are very difficult to identify in MPM images because the source of contrast is the same: melanin fluorescence. But they can be distinguished by their morphology. Nevus cells form nests at the EDJ or in the dermis, as shown

in Figure 2 (d-f). These images show a well-defined nest as the cluster of nevus cells is completely surrounded by collagen fibers.

Corresponding F values for the images that were included in the quantitative analysis and the S value for the full image stack are reported in the legend of Figure 2.

Dysplastic nevi

We imaged 5 dysplastic nevi with varying degrees of atypia. At least one of the following features was present in the MPM images: mild cellular atypia (enlarged nuclei), lentiginous hyperplasia (nevus cells with dense distribution along the basal layer), acanthosis (thickening of the epidermal layer), occasional melanocytes in the stratum spinosum and nevus cells distributed in nests that were irregular in both shape and distribution along the EDJ. The thickness of the epidermis was estimated by the depth at which the EDJ was visualized in the stack of images acquired from the stratum corneum to superficial dermis. Melanocytic dendrites in the spinosum layer of the epidermis could be visualized in two out of five dysplastic nevi imaged (Figure S2). Mild cytological atypia and mild architectural disorder were also identified in these lesions. Mean F and S values for dysplastic nevi ranged between 0.78 - 1.05 and 0.37 - 0.53, respectively. The mean D values ranged between zero and 7800 dendrites/mm^3 (Table 1).

Representative MPM images of a dysplastic nevus along with corresponding histology are shown in Figure 3. The histopathologic diagnosis was compound dysplastic nevus with mild atypia. The MPM images of the lesion showed lentiginous hyperplasia and irregular nests of nevus cells along the basal layer and in the papillary dermis. There was also more variability in cell size compared with common nevi.

Corresponding F values for the images that were included in the quantitative analysis and the S value for the full image stack are reported in the legend of Figure 3. The D value was zero for this lesion.

Melanoma

We imaged 5 patients who were diagnosed with melanoma corresponding to two sub-types of melanoma: superficial spreading melanoma (3) and lentigo maligna type (2).

In superficial spreading melanoma lesions, we imaged proliferation of atypical melanocytes (highly pleomorphic melanocytes) at all levels within the epidermis and Pagetoid spread (presence of melanocytes within the upper portion of the epidermis singly or in groups) (Figure S3). In melanoma lentigo malignant type lesions, we imaged atypical melanocytes in upper epidermal layers and invasion of melanoma cells in the dermis. Mean F and S values for melanoma lesions ranged between 0.58 - 0.8. and 0.06 - 0.38, respectively. The mean D values ranged between 8500 dendrites/mm^3 and 78000 dendrites/mm^3 (Table 1).

MPM and histology images from one of the superficial spreading melanomas are shown in Figure 4. MPM images of the lesion showed the presence of melanocytic dendrites in the upper layers of the epidermis (Figure 4c), proliferation of atypical melanocytes, and architectural disorder in the basal layer (Figure 4d-f). Melanoma cells and suspected melanophages can be visualized in the dermis (Figure 4f). These features correlate well with the ones found in the corresponding histologic sections of the lesion (Figure 4b). F values for the images that were included in the quantitative analysis and the S value for the stack the images belong to are reported in the legend of Figure 4. The mean D value for this lesion was 63878 dendrites/mm^3.

The ranges of the mean F, S and D values corresponding to the pigmented lesions in different stages were summarized in Table 1. The distribution of the mean values of the quantitative parameters F, S and D are plotted in Figure 5a-c. Significant differences between mean values for each group were evaluated using the Mann-Whitney U test. The null-hypothesis was that the mean F, S, and D parameters were the same for two different groups. We rejected the null-hypothesis for a U value ≤ 2 (the critical value for our experimental conditions), corresponding to $p<0.05$. Evaluating the U values for each pair of groups, we found 1) the mean values of the F parameter corresponding to melanoma were significantly different from the mean values for dysplastic and common nevi ($p=0.016$ and 0.009, respectively). Common and dysplastic nevi were not distinguished by the mean F parameter ($p=0.5$). 2) The mean values of the S parameter for each group were significantly different from the values of the other two groups (p values between 0.009 and 0.016). 3) Parameter D separated significantly melanoma from common and dysplastic nevi ($p=0.009$), but did not distinguish between common and dysplastic nevi ($p=0.3$).

The correlation between each of the parameters F, S and D is shown in Figure 5 e-g. In this figure, the combination (color, marker) corresponds to an individual lesion. It can be noted, for example, that the dysplastic nevus with the maximum value of D (blue triangle, solid arrows) -closest to melanoma- also has the minimum value of S, and a value of F close to minimum. In fact, from the dysplastic nevi we imaged, this was the only one diagnosed as nevus with 'moderate to severe' dysplasia. One of the lesions diagnosed as 'lentigo maligna' corresponds to the red circle in Figure 5 e-g (dashed arrows). In this lesion we imaged only occasional ascending melanocytes in the upper epidermal layers (low D value), but severe proliferation of atypical melanocytes at the EDJ and invasion in the dermis. Melanocytic proliferation resulted

in a high degree of homogeneity in the intensity of the TPEF images (low F value) due to a more uniform, increased pigmentation. The S value (a measurement of dermal invasion) for this lesion was low, but not minimum. Figures 5e and f and the calculated Pearson correlation coefficients (ρ) show that the S and F parameters are weakly correlated with D (ρ=-0.47, p=0.074 for S and D; ρ=-0.5, p=0.057 for F and D), while in 5g we see that S and F are well correlated with each other (ρ=0.71, p=0.0032). The relationship between S and F is not surprising given the fact that they sample similar regions and complementary processes around the EDJ. Among the three parameters, S is the only one that can fully resolve all the three states (i.e. benign, dysplastic, malignant). However, a combination of all three parameters improves the performance by increasing the separation between the dysplastic and melanoma groups, which we are mostly concerned about (the p value is reduced from 0.016 to 0.009). Therefore, in order to increase the performance of the metrics F, S and D, we assigned each of these criteria a histologic score from 0 to 3 on the basis of visualizing the mean values, as shown in Figure 5 a-c and Table 2. For each lesion, the scores of the three criteria were summed up to give a final continuous MMI index, ranging from 0 to 9. Using this approach, common nevi scored between 0 and 1, dysplastic nevi between 1 and 4 and melanoma between 5 and 8. The distribution of these scores for the three groups is shown in Figure 5d. Mann Whitney U test shows that the MMI scores corresponding to melanoma group are significantly different from the other two groups (p=0.009). The difference in MMI scores of common and dysplastic nevi is marginally significant (p=0.03).

DISCUSSION

MPM is capable of non-invasive *in vivo* imaging of human skin with sensitivity to the epidermis and superficial dermis (9). In this study we performed qualitative and quantitative

analysis of melanocytic nevi at three stages: common nevi with no dysplastic changes, dysplastic nevi, and melanoma. The qualitative analysis involved identifying morphological features of the lesions in the three groups and correlating MPM with histologic features. The quantitative analysis was based on TPEF, SHG, and melanocyte parameters derived from 3D *in vivo* image analysis.

Common melanocytic nevi were characterized in MPM images by normal morphology of keratinocytes of the epidermal layers, well-defined nests of nevus cells surrounded by collagen fibers at the EDJ and dermis, and elongated rete ridges.

MPM images of dysplastic nevi showed lentiginous hyperplasia, mild cellular atypia, and nests of nevus cells that were less defined and more irregular in shape and distribution than the nests imaged in common melanocytic nevi. The presence of melanocytic dendrites in the stratum spinosum of the epidermis was revealed in two of five dysplastic nevi. We found that this feature requires careful evaluation in order to avoid false-positive diagnosis, as migration of melanocytes into the upper layers of epidermis is a feature also present in melanoma.

Although migration of melanocytes in the upper layers of the epidermis usually raises suspicion of melanoma, limited migration of melanocytes in the stratum spinosum of the epidermis is acceptable in dysplastic nevi (18). In this case, the architectural disorder influences the overall grade. Indeed, in the lesions characterized by ascending melanocytes in the spinosum layer of the epidermis and diagnosed as dysplastic nevi by histopathology, MPM architectural disorder was milder in comparison with histopathologically-confirmed melanoma.

In the pigmented lesions diagnosed as melanoma by histopathology, cytological atypia and architectural disorder were the main features revealed by *in vivo* MPM imaging. This finding is in good agreement with histopathology and the MPM diagnosis criteria identified in a previous

study (12). In addition, we identified specific MPM features characteristic of two melanoma sub-types: 1) superficial spreading melanoma where epidermis is mainly involved and there is proliferation of melanocytes and pleomorphic cells (Pagetoid spread) throughout all epidermal layers, and 2) lentigo maligna melanoma where the basal layer rather than the epidermis is mainly affected, atypical melanocytes were more confined to the basal layer, and there was less Pagetoid spread in the upper epidermal layer along with epidermal atrophy.

Most of the histologic criteria for diagnosis of dysplastic nevi and melanoma, such as cellular atypia, lentiginous hyperplasia, elongated dermal papilla, ascending melanocytes, and Pagetoid spread were identified by MPM. Other histologic criteria cannot be easily identified in MPM images and they would need to be correlated with MPM content. For instance, nests of nevus cells localized on the sides of dermal papilla in histologic images of dysplastic nevi are difficult to visualize in the MPM horizontal (i.e. x-y or *en face*) optical sections. These histologic features can be seen in MPM images as nests of nevus cells, irregular in size and distribution, along the basal layer and in the dermis. Common nevi were not biopsied, but we anticipate that nests of nevus cells localized at the tips of the rete ridges in the histologic images of common nevi are related to well-defined regular nests of nevus cells surrounded by collagen fibers in the MPM images.

Morphological changes such as cytological atypia and lentiginous hyperplasia correlate with the TPEF signal. Likewise, morphological changes at the EDJ such as appearance of nests of nevus cells on the sides of the rete ridges or disruption of the junction correlate with variations in the SHG signal. TPEF and SHG are most sensitive to these processes when measured over a volume of the EDJ, i.e. several x-y image planes, in the region of early stage melanoma genesis. In the TPEF images corresponding to the three groups of lesions: common, dysplastic and

melanoma, we identified a variation in the ratio of the spatial standard deviation and the mean pixel intensity for the different groups. This ratio (the F score) measured over a stack of images (see Methods), is related to the degree of pixel intensity homogeneity in the image. MPM images of melanoma lesions showed a higher degree of homogeneity due to a more uniform, increased pigmentation in the EDJ area. The mean F ratios measured in melanomas were significantly lower than the ratios measured in common ($p=0.009$) and dysplastic nevi ($p=0.016$). The mean ratios corresponding to common nevi and dysplastic nevi did not show a statistically significant difference ($p=0.5$).

In the SHG images of the three groups of lesions, we identified a variation in the ratio of the standard deviation and the mean density of the bright pixels in the SHG binary images across a stack of images corresponding to EDJ. This ratio (the S score) is related to the change in collagen amount across the EDJ. A large ratio reflects a rapid increase in the collagen amount from the top of the dermal papilla to deeper layers in the papillary dermis. Large ratios were characteristic of common nevi. Low ratios, which reflect a slower increase in collagen content across the junction, are due to the presence of cells in the papillary dermis; typically nevus cells from the sides of the rete ridges in dysplastic nevi and melanocytes in melanoma lesions. The mean values of these ratios corresponding to each group were significantly different from the values of the other two groups (p values between 0.009 and 0.016).

A third measureable criterion for distinguishing dysplastic nevi from melanoma, the D score, is related to the density of melanocytic dendrites in the upper epidermal layers. Dysplastic nevi were characterized by significantly lower density of melanocytic dendrites in the upper epidermal layers compared to melanoma lesions. By combining melanocyte morphology with TPEF and SHG features, we developed a quantitative 0-9 point algorithm for evaluating in vivo

images, structured in a manner similar to well-established histology scoring methods such as the Bloom-Richardson grading system (19). This integrated "multi-photon melanoma index" (MMI) assigns unique values to each lesion. By having a continuous 9-point scale, it is possible to separate common nevi (MMI = 0–1), dysplastic nevi (MMI = 1-4) and melanoma (MMI = 5-8) with a high degree of statistical significance (p values between 0.009 and 0.03). Given the relatively small sample size we feel that the 3 parameters F, S and D, which sample different but complementary physiological processes, are useful in describing a quantitative melanoma index. However as our patient population expands it is possible that sufficient predictive power can be achieved in future studies with a subset of these parameters.

The results of this study provide an initial set of MPM features that are characteristic of common nevi, dysplastic nevi, and melanoma and correspond to descriptions from conventional histopathology. Using these criteria we, we have developed, for the first time, a quantitative algorithm derived from *in vivo* MPM measurements that shows potential to discriminate between these groups of melanocytic lesions. These results are certainly limited by the small number of subjects. Dysplastic nevi, in particular, have very diverse features and a larger population is necessary to validate diagnostic performance. Nevertheless, these findings and previously reported results (12) identify MPM signals that are consistent with melanoma and could be used to help guide further investigations. A more comprehensive study of a larger number of patients is necessary in order to validate the proposed scoring algorithm and evaluate how well MPM technology can distinguish dysplastic nevi from common nevi and melanoma. This could help dermatologists increase the accuracy of their diagnosis for pigmented lesions that fall into the borderline area, minimize the need for invasive biopsies, and advance our knowledge of

underlying biological factors that influence the appearance and progression of melanoma and related skin diseases.

Acknowledgements

Support for this work was provided by the National Institutes of Health (NIH) NIBIB Laser Microbeam and Medical Program (LAMMP, P41-EB015890), NCI-2P30CA62203 (University of California, Irvine Cancer Center Support Grant) and NIH K25-EB007309. Beckman Laser Institute programmatic support from the Arnold and Mabel Beckman Foundation and Air Force Research Laboratory Agreement No. FA9550-04-1-0101 is acknowledged.

References

1. Siegel R, Naishadham D, Jemal A. Cancer statistics, 2012. CA Cancer J Clin. 2012;62:10-29.
2. Howlader N, Noone A, Krapcho M, Neyman N, Aminou R, Waldron W, et al. SEER Cancer Statistics Review, 1975-2008: National Cancer Institute. Bethesda, MD, http://seer.cancer.gov/csr/1975_2008/, based on November 2010 SEER data submission, posted to the SEER web site, 2011; 2011.
3. Balch CM, Gershenwald JE, Soong SJ, Thompson JF, Atkins MB, Byrd DR, et al. Final version of 2009 AJCC melanoma staging and classification. Journal of clinical oncology : official journal of the American Society of Clinical Oncology. 2009;27:6199-206.
4. Abbasi NR, Shaw HM, Rigel DS, Friedman RJ, McCarthy WH, Osman I, et al. Early diagnosis of cutaneous melanoma - Revisiting the ABCD criteria. Jama-J Am Med Assoc. 2004;292:2771-6.
5. Osborne JE, Bourke JF, Graham-Brown RA, Hutchinson PE. False negative clinical diagnoses of malignant melanoma. Br J Dermatol. 1999;140:902-8.
6. Osborne JE, Chave TA, Hutchinson PE. Comparison of diagnostic accuracy for cutaneous malignant melanoma between general dermatology, plastic surgery and pigmented lesion clinics. Brit J Dermatol. 2003;148:252-8.
7. Koh HK, Norton LA, Geller AC, Sun T, Rigel DS, Miller DR, et al. Evaluation of the American Academy of Dermatology's national skin cancer early detection and screening program. J Am Acad Dermatol. 1996;34:971-8.
8. Langley RG, Rajadhyaksha M, Dwyer PJ, Sober AJ, Flotte TJ, Anderson RR. Confocal scanning laser microscopy of benign and malignant melanocytic skin lesions in vivo. J Am Acad Dermatol. 2001;45:365-76.

9. Konig K, Riemann I. High-resolution multiphoton tomography of human skin with subcellular spatial resolution and picosecond time resolution. J Biomed Opt. 2003;8:432-9.
10. Matthews TE, Piletic IR, Selim MA, Simpson MJ, Warren WS. Pump-probe imaging differentiates melanoma from melanocytic nevi. Sci Transl Med. 2011;3:71ra15.
11. Krasieva TB, Stringari C, Liu F, Sun CH, Kong Y, Balu M, et al. Two-photon excited fluorescence lifetime imaging and spectroscopy of melanins in vitro and in vivo. J Biomed Opt. 2013;18:031107.
12. Dimitrow E, Ziemer M, Koehler MJ, Norgauer J, Konig K, Elsner P, et al. Sensitivity and Specificity of Multiphoton Laser Tomography for In Vivo and Ex Vivo Diagnosis of Malignant Melanoma. J Invest Dermatol. 2009;129:1752-8.
13. Lever WF, Schaumburg-Lever G. Histopathology of the skin-Sixth Edition: Melanocytic Nevi and Malignant Melanoma: Lippincott Williams and Wilkins; 1990.
14. McKee PH, Calonje E, Granter SR. Pathology of the Skin: Melanocytic nevus. 3rd ed: Mosby; 2005.
15. Rasband WS. ImageJ, U. S. National Institutes of Health, Bethesda, Maryland, USA. 1997-2012 http://imagej.nih.gov/ij/
16. http://rsbweb.nih.gov/ij/docs/faqs.html - auto
17. Meijering E, Jacob M, Sarria JC, Steiner P, Hirling H, Unser M. Design and validation of a tool for neurite tracing and analysis in fluorescence microscopy images. Cytometry A. 2004;58:167-76.
18. Culpepper KS, Granter SR, McKee PH. My approach to atypical melanocytic lesions. J Clin Pathol. 2004;57:1121-31.
19. Bloom HJ, Richardson WW. Histological grading and prognosis in breast cancer; a study of 1409 cases of which 359 have been followed for 15 years. Br J Cancer. 1957;11:359-77.

Table Legends

Table 1. The mean values of the quantitative parameters F, S, D corresponding to the three stages of the pigmented lesions: common, dysplastic nevi and melanoma

Table 2. Scoring system based on visualizing the mean values of the parameters F, S, D plotted in Figure 5.

Figure Legends

Figure 1. Pigmented normal skin. (Left) Horizontal sections of MPM images (XY scans) at different depths showing images of the stratum corneum (z=0μm), keratinocytes normally distributed in the stratum spinosum (z=25μm), the basal cells (green) surrounding dermal papilla (blue) (z=50μm), collagen fibers (blue) and cross-sections of blood vessels (white arrows) (z=75μm), collagen (blue) and elastin (green) in the dermis (z=120μm). **(Right)** Cross-sectional view (XZ scan) corresponding to a vertical plane through the horizontal sections on the left. Arrows point to blood vessels.

Figure 2. Compound nevus. (a) Clinical image (DermLite FOTO, Dermlite Inc.) **(b)** MPM image of the basal layer showing nevus cells and pigmented basal cells; F=1.02 **(c)** MPM image of the basal layer showing nevus cells, pigmented basal cells (green) and appearance of dermal papilla (blue); F=1.04 **(d)** MPM images showing a nest of nevus cells (green) surrounded by collagen (blue) fibers; F=0.95 **(e-f)** MPM images at different depths showing a nest of nevus cells (green) surrounded by collagen (blue) and elastin (green) fibers. The S value for this stack is 0.51. Scale bar is 40 μm.

Figure 3. Dysplastic nevus. Clinical image (DermLite FOTO, Dermlite Inc.) **(a)** Histologic section of the lesion **(b)** MPM images showing irregular nests of nevus cells (green) and collagen fibers (blue) along the basal layer at depths of 30 μm **(c)**, 40 μm **(d)**, 50 μm **(e)** and 60 μm **(f)**. The corresponding F values are 0.89 **(c)** and 0.86 **(d)**. The S value for this stack is 0.41. Scale bar is 40 μm.

Figure 4. Melanoma - superficial spreading type. (a) Clinical image (DermLite FOTO, Dermlite Inc.) **(b)** Histologic section of the lesion **(c)** MPM images showing ascending melanocytes (arrows) in the granulosum layer of the epidermis **(d)** MPM images of the basal layer showing proliferation of atypical melanocytes (highly pleomorphic melanocytes) F=0.69 **(e-f)** MPM images of the basal layer showing basal cells and atypical melanocytes (green) surrounding dermal papilla (blue); F=0.63 and 0.62 respectively **(g)** MPM images showing melanoma cells and probably melanophages invading the dermis (blue-collagen fibers). The S value for this stack is 0.35. Scale bar is 40 μm.

Figure 5. Distribution and correlation of the mean values and scores. The distribution of the mean values of F **(a)**, S **(b)** and D **(c)** parameters for common nevi, dysplastic nevi and melanoma. **(d)** The distribution of the MMI scores for common nevi, dysplastic nevi and melanoma. **(e-g)** Correlation of F, S and D values. The combination (color, marker) corresponds to an individual lesion. Black, blue and red represent the 'common nevi', the 'dysplastic nevi' and the 'melanoma' groups, respectively. Arrows point to the markers corresponding to the lesions discussed in the text.

Table 1. The mean values of the quantitative parameters F, S, D corresponding to the three stages of the pigmented lesions: common, dysplastic nevi and melanoma

	Common	Dysplastic	Melanoma
<F>	0.86-1.07	0.78-1.05	0.58-0.8
<S>	0.42-0.6	0.37-0.53	0.06-0.38
$<Dx10^3>$	0	0-7.8	8.5-78

Table 2. Scoring system based on visualizing the mean values of the parameters F, S, D plotted in Figure 5.

	0	**1**	**2**	**3**
<F>	>0.9	0.8-0.9	0.7-0.8	<0.7
<S>	>0.5	0.4-0.5	0.3-0.4	<0.3
$<Dx10^3>$	<1	1-20	20-40	>40

Figure 1

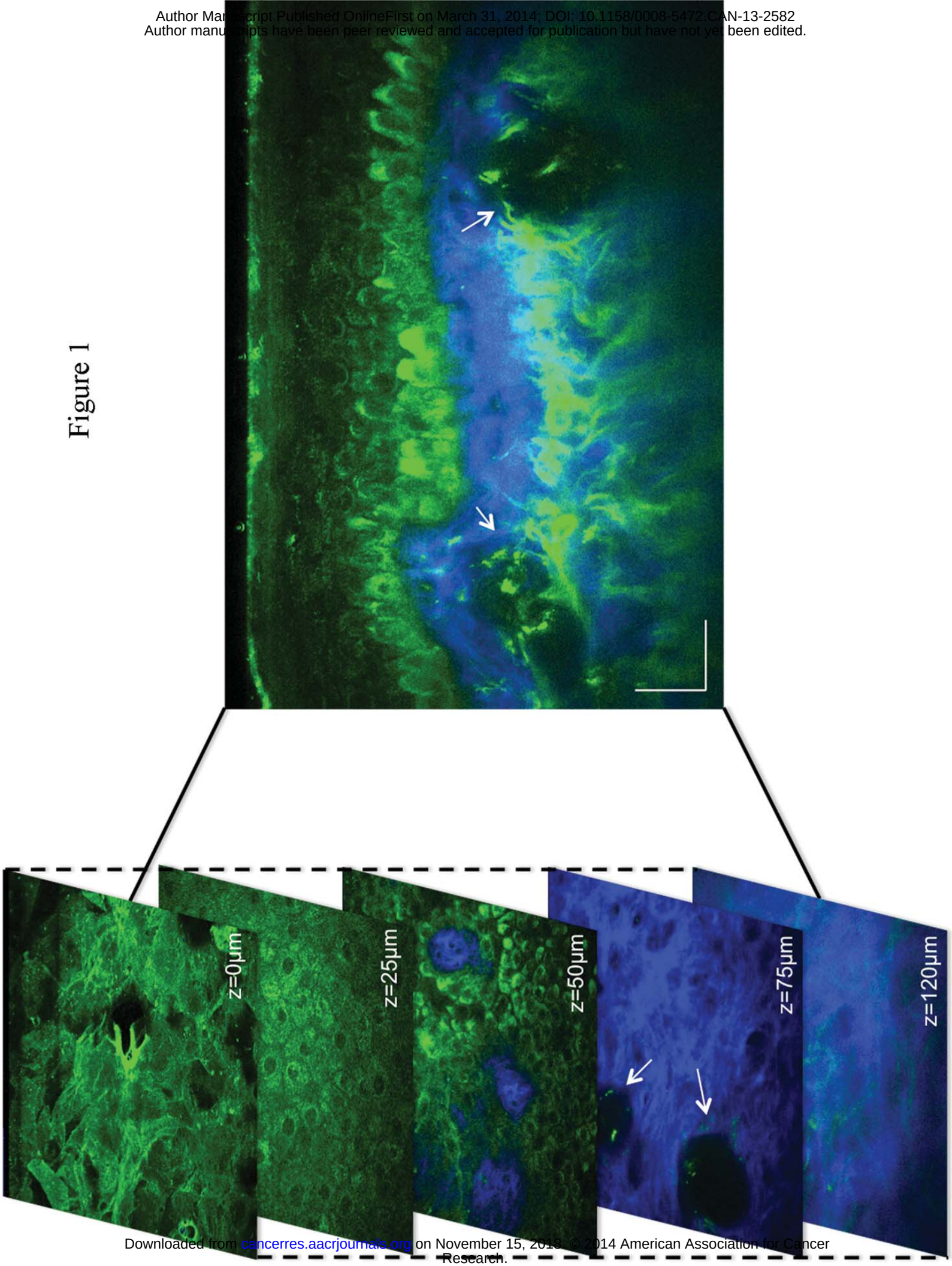

Figure 2

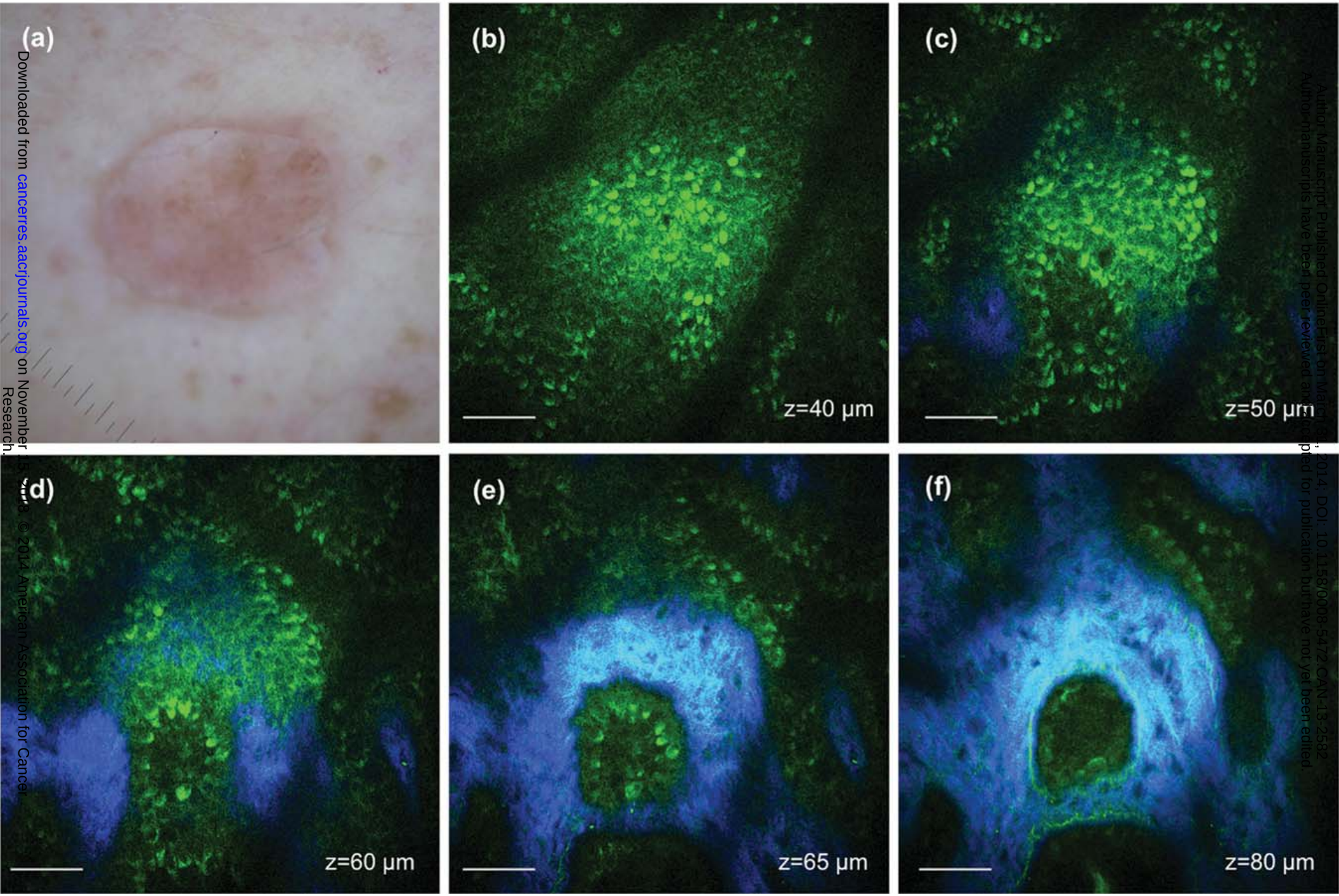

Figure 3

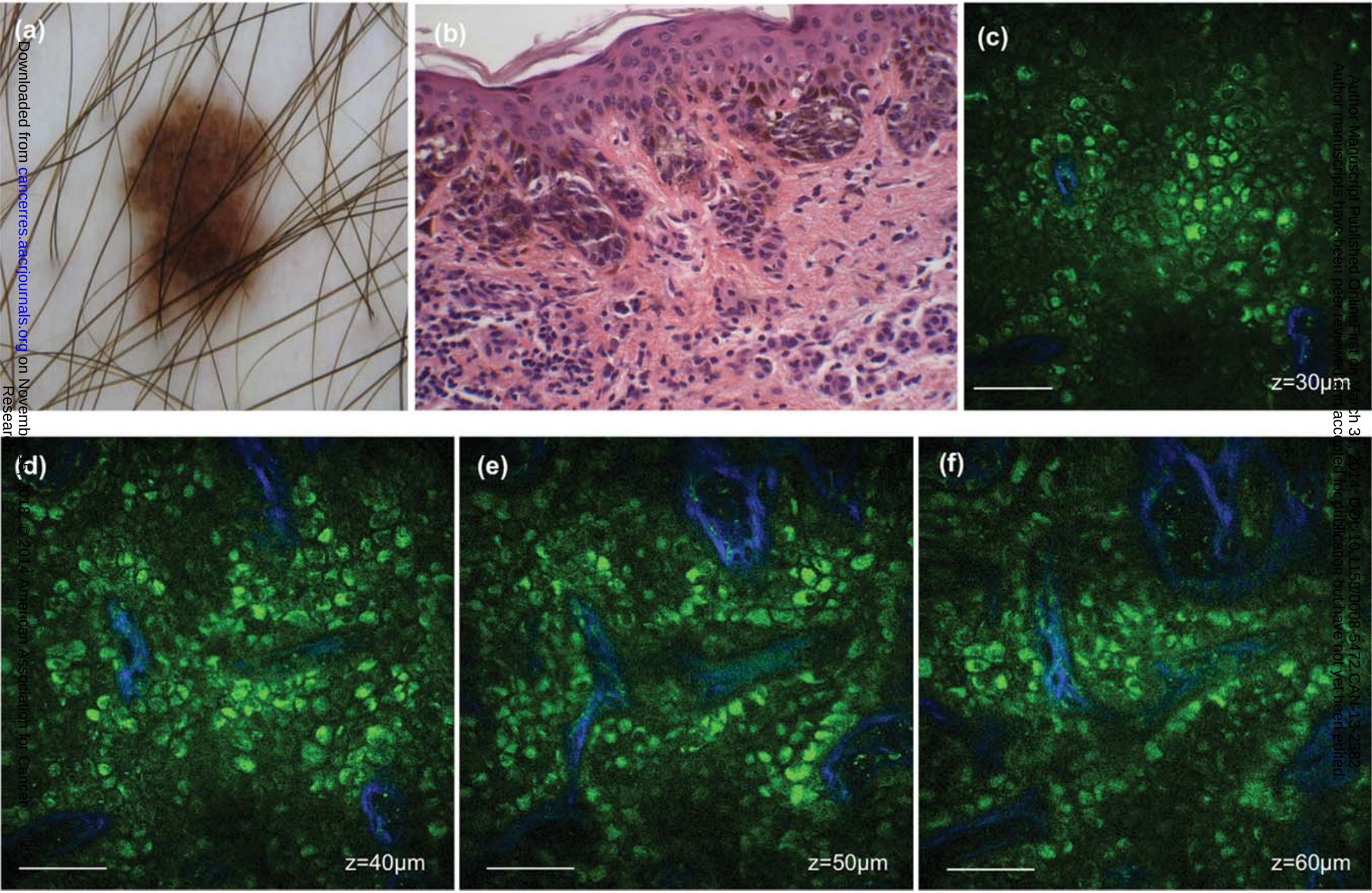

Figure 4

Figure 5

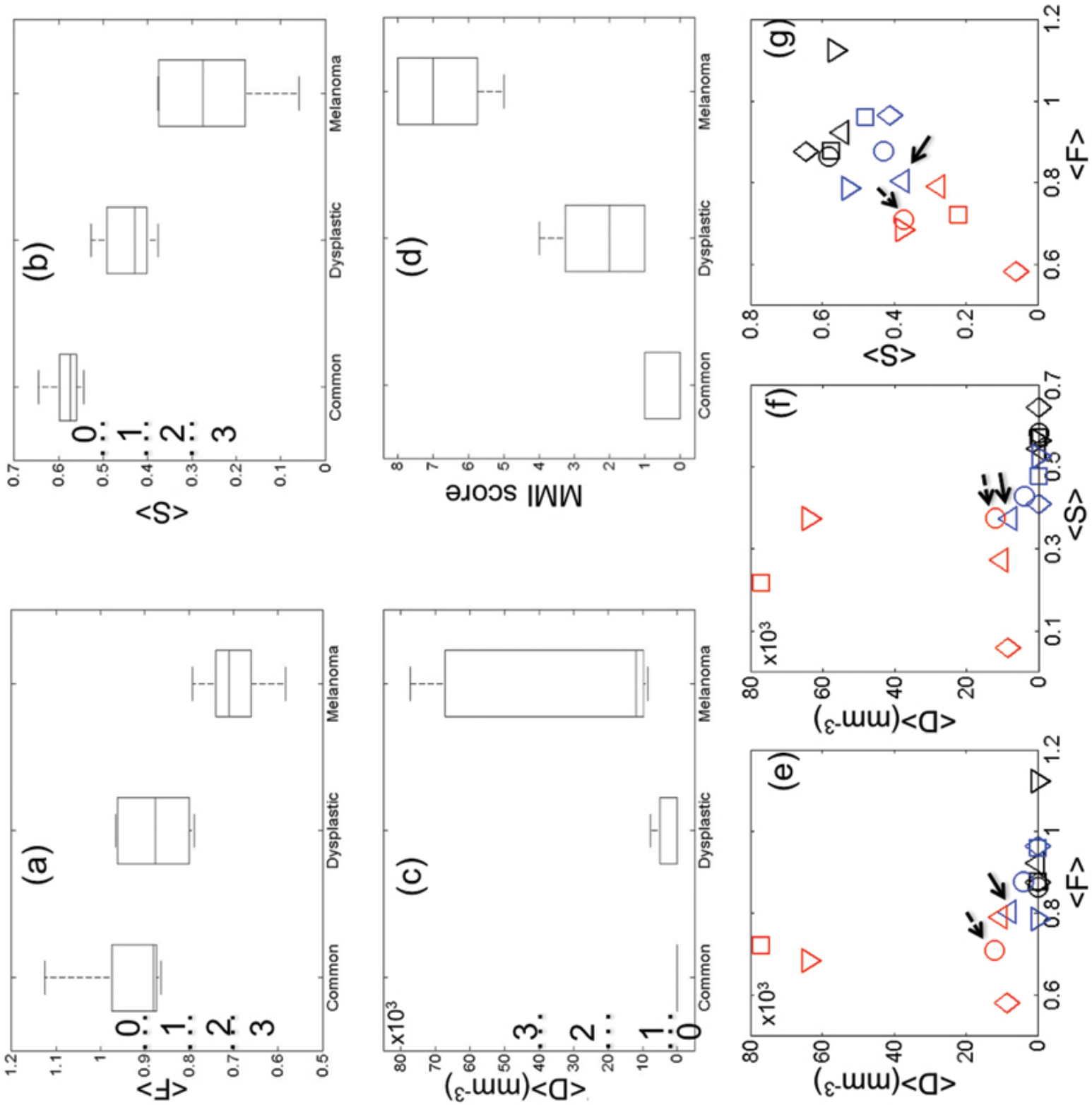

AACR American Association for Cancer Research

Cancer Research

The Journal of Cancer Research (1916–1930) | The American Journal of Cancer (1931–1940)

Distinguishing between benign and malignant melanocytic nevi by in vivo multiphoton microscopy

Mihaela Balu, Kristen M. Kelly, Christopher B. Zachary, et al.

Cancer Res Published OnlineFirst March 31, 2014.